

Analysis of heat transfer in deformed liver cancer modeling treated using a microwave coaxial antenna

P. Keangin, T. Wessapan, P. Rattanadecho*

Research Center of Microwave Utilization in Engineering (R.C.M.E.), Department of Mechanical Engineering, Faculty of Engineering, Thammasat University (Rangsit Campus), Pathumthani 12120, Thailand

ARTICLE INFO

Article history:

Received 30 July 2010

Accepted 2 June 2011

Available online 12 June 2011

Keywords:

Liver cancer

Microwave ablation

Thermal expansion

ABSTRACT

In interstitial microwave ablation (MWA), cancer is treated by applying localized heating to the tumor tissue. Some of the challenges associated with the selective heating of cancer cells, without damaging the surrounding tissue, entail a control of heating power for appropriate temperature distribution. This paper is carried out on the computer simulation of liver cancer treated using a microwave coaxial antenna (MCA). The mathematical models consist of a coupled electromagnetic wave equation, bioheat equation and mechanical deformation equation. In numerical simulation, these coupled mathematical models are solved by using an axisymmetric finite element method (FEM) with temperature dependent thermal and dielectric properties to describe the microwave power absorbed, specific absorption rate (SAR) distribution, temperature distribution and strain distribution in liver tissue. The comparison of the simulated results in model with and without deformation is also considered in order to approach realistic tissue modeling. The results show that the model with deformation, which is the more accurate way to simulate the physical characteristics of therapeutic liver cancer compared to the literature results and hence leads to more useful in the medical approach.

© 2011 Elsevier Ltd. All rights reserved.

1. Introduction

Microwave is a one heat source that is an attractive alternative over conventional heating methods because an electromagnetic wave that penetrates the surface is converted into thermal energy within the material. High speed startup, selective energy absorption, instantaneous electric control, non-pollution, high energy efficiency, and high product quality are several advantages of microwave heating. Therefore, these technologies have been used in many industrial and household applications. For example, food industry for drying, pasteurization, sterilization, etc. [1]. Other uses include, heating process [2], vulcanization processing, curing of cement [3], melting of frozen products [4], drying of foods [5] and drying of textiles. Recently, microwave has been introduced as a rapid method of delivering high temperatures to destroy the cancer cells.

Liver cancer is a significant worldwide public health issue. The disease has a mortality rate of 100% at 5 years in untreated cases [6] and results in the deaths of more than one million people each year

worldwide [7]. In this past, possible treatments for liver cancer are surgical resection, cryosurgery, chemotherapy, radiation and radiofrequency ablation (RFA) [8]. Each therapy method is limited by the side effects of the treatment. There are many types of new technologies to reduce the injury effects. One promising alternative liver cancer treatment is microwave ablation (MWA), using microwaves. The energy from the microwave frequency waves emitted by the microwave coaxial antenna (MCA) creates heat in the local cancerous tissue cancer without damaging the surrounding tissue. MWA is a minimally invasive modality for the local treatment of solid tumors and can also enhance the effects of certain anticancer drugs [9]. In addition, MWA results in a large zone of active heating to the liver tissue.

The experimental cancer therapy cannot be carried out on live human beings. Consequently, there are experimental studies in animals [10]. However, they may not represent a realistic situation of cancer treatment. Therefore, the modeling of MWA in biological tissue is needed. Most studies used bioheat equation for heat transfer analysis. Pennes's bioheat equation, introduced by Pennes [11] based on the heat diffusion equation, is a frequency used for analysis of heat transfer in biological tissues. The studies of high temperatures tissue ablation using a modified bioheat equation to include tissue internal water evaporation during heating have

* Corresponding author. Tel.: +66 2 564 3001 9x3153; fax: +66 2 564 3010.

E-mail address: ratphadu@engr.tu.ac.th (P. Rattanadecho).

been proposed [12]. The simulation result is found in agreement with experimental results. Okajima et al. [13] derived the dimensionless steady-state solutions of bioheat transfer equation to discuss the bioheat transfer characteristics common to all organs or tissues. Chua and Chou [14] have developed a bioheat model to study the freeze–thaw thermal process of cryosurgery. Many studies have been conducted using the coupled model of the bio-heat equation and electromagnetic wave equation [15,16]. By using the model, in the area of antenna design, several researchers have numerically modeled and studied the performance of the designed antenna [17,18]. At present, there are three principal techniques that exist within computational electromagnetic (CEM); the finite-difference time-domain (FDTD) method, the method of moments (MOM), and the finite element method (FEM). FEM has been extensively used in simulations of cardiac and hepatic RFA process [19]. Moreover, FEM models can provide users with quick, accurate solutions to multiple systems of differential equations, and as such, are well suited to heat transfer problems like ablation process.

In reality, when biological tissue gains heat from an outer heat source, its shape is deformed and induced thermal strain in the biological tissue. There was a research which presents a coupled model of bioheat transfer and a mechanical deformation in biological tissue to obtain quantitative descriptions of thermo-mechanical behavior of biological tissue [20]. Some work has been done in the simulation of thermomechanical response in skin under medical electromagnetic heating [21]. Nevertheless, most of the studies have concentrated on only electromagnetic wave propagation and heat transfer however do not consider tissue mechanical deformation. There is a little work in MWA that presented the complete mathematical model considered the coupled model of electromagnetic wave propagation, heat transfer and mechanical deformation in biological tissue in the couple way. This is useful for the development of biomedical technologies especially.

The ultimate goal of ablation technology, considering MWA, is to kill the liver cancer cells, while effectively preserving the healthy liver tissue. Clinical treatment with MWA needs to control the tissue temperature and the lesion generation accurately, in order to ensure cancer cells destruction and to minimize side effects to surrounding tissue and surrounding organs. Heat elevations are a direct consequence of altered thermal balance resulting from metabolic and externally applied heat source [22]. Even relatively small increases in body temperature, as well as thermal deformation, lead to such effects as altered production of hormones, suppressed immune response, and protein denaturation [23]. Therefore, comprehension of the phenomena of heat transfer and mechanical deformation of liver tissue under these medical treatments can contribute to a variety of medical application. In order to describe MWA adequately, a mathematical model that includes the mechanical behavior of tissue is needed to represent the actual process of heat transfer in human tissue. It is essential to study the coupled electromagnetic wave propagation, heat transfer, and mechanical deformation of the tissue for effective treatment.

In this study, the influence of mathematical models in model with and without deformation on microwave power absorbed, SAR distribution, temperature distribution and strain distribution in liver tissue during MWA, is investigated systematically. Mathematical models based on coupled equations of electromagnetic wave equation, bioheat equation and mechanical deformation equation are solved by using an axisymmetric FEM. The comparison of the present simulated results with the simulated and experimental results obtained by Yang et al. [12] is also considered in order to test the efficiency of the proposed model. The simulated results in this study can be used as a guideline for the practical treatment.

2. Problem statement

This study uses a single slot MCA, to transfer microwave power into liver tissue for the treatment of liver cancer. The MCA has a diameter of 1.79 mm because the thin antenna is required in the interstitial treatments. A ring-shaped slot, 1 mm wide is cut off the outer conductor 5.5 mm in length from the short-circuited tip because the effective heating around the tip of the antenna is very important to the interstitial heating and because the electric field becomes stronger near the slot. The MCA are composed of an inner conductor, a dielectric and an outer conductor. The MCA are enclosed in a catheter (made of polytetrafluorethylene; PTFE), for hygienic and guidance purposes. Fig. 1 shows the model geometry of an MCA. The MCA operates at the frequency of 2.45 GHz, a widely used frequency in MWA, and the input microwave power is 10 W. The goal of MWA is to elevate the temperature of un-wanted tissue to 50 °C where cancer cells are destroyed [24]. Dimensions of the MCA are given in Table 1.

The liver tissue is considered as a cylindrical geometry. It has a 30 mm radius and 80 mm in height and an MCA is inserted into the liver tissue with 70.5 mm depth as shown in Fig. 2. An axially symmetric model is considered in this study, which minimized the computation time while maintaining good resolution and represents the full three-dimensional result. The model assumes that the MCA is immersed in a homogeneous smooth biological tissue. The vertical axis is oriented along the longitudinal axis of the MCA, and the horizontal axis is oriented along the radial direction.

The physical properties of the materials involved in the model are selected from several literatures; [12,21,25–27]. The thermal properties, dielectric properties and mechanical properties of liver tissue and MCA are given in Table 2 considered at frequency of 2.45 GHz.

3. The formulation of the mathematical model

A mathematical model has been formulated to predict the microwave power absorbed, SAR distribution, temperature distribution and strain distribution in liver tissue under the MWA process. As a rudimentary step of the study, some assumptions are made to simplify the analysis. The liver tissue is the homogeneous

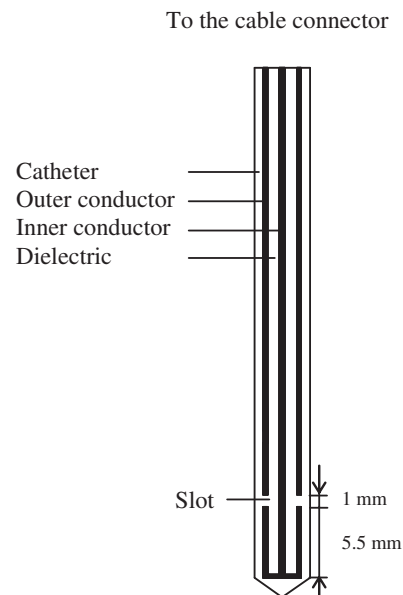


Fig. 1. Model geometry of an MCA.

Table 1
Dimensions of an MCA.

Materials	Dimensions (mm)
Inner conductor	0.135 (radial)
Dielectric	0.335 (radial)
Outer conductor	0.460 (radial)
Catheter	0.895 (radial)
Slot	1.000 (wide)

biomaterial. In the electromagnetic wave propagation analysis, a scattering boundary condition is set on that surface, which means that the boundary does not disturb the electromagnetic field distribution. The microwave source is set at the upper end of the MCA and the input microwave power emitted is adjusted to 10 W. An electromagnetic wave, propagating in an MCA, is characterized by transverse electromagnetic fields (TEM) [26]. In the liver tissue, an electromagnetic wave is characterized by transverse magnetic fields (TM) [26]. The model assumes that the wall of the MCA is a perfect electric conductor, and the dielectric properties of liver tissue have been determined as a function of temperature. While in the heat transfer analysis, temperature-dependent properties are considered for the thermal properties. No phase change occurs within the liver tissue, no energy exchange through the outer surface of liver tissue, and no chemical reactions occur within the liver tissue. The outer surface between the MCA and liver tissue is considered as insulation boundary condition. In mechanical deformation analysis, the outer liver tissues are moving surface boundary as a result of thermal strain. The liver tissue connected to the MCA, are set to fixed surface boundary. The relevant boundary conditions are described in Fig. 3.

3.1. Electromagnetic wave propagation analysis

The axisymmetric FEM model used in this study is adapted from an MCA general model [12,28]. In this model, the electric and magnetic fields associated with the time-varying TEM wave are expressed in 2D axially symmetrical cylindrical coordinates:

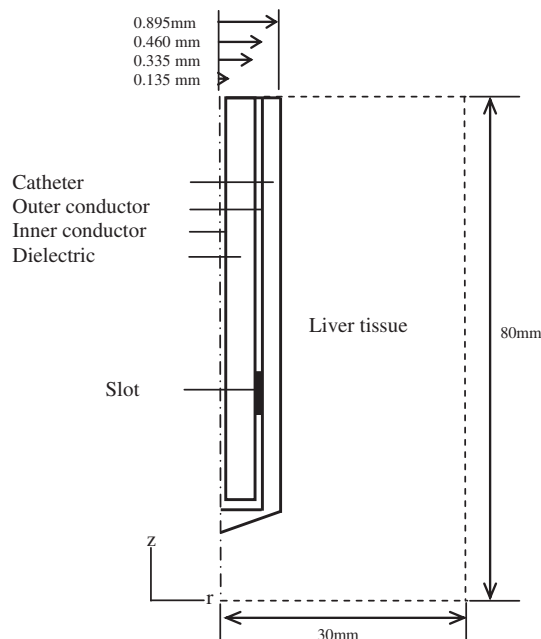


Fig. 2. Axially symmetrical model geometry.

Table 2
Properties of liver tissue and microwave coaxial antenna.

Parameters	Values	Parameters	Values
Properties of liver tissue		Properties of microwave coaxial antenna	
Density of blood; ρ_b	1060 kg/m ³	Relative permittivity of dielectric; $\epsilon'_{r,die}$	2.03
Specific heat capacity of blood; C_b	3600 J/kg °C	Electric conductivity of dielectric; σ_{die}	0 S/m
Blood temperature; T_b	37 °C	Relative permeability of dielectric; $\mu_{r,die}$	1
Relative permeability of liver; $\mu_{r,liver}$	1	Relative permittivity of catheter; $\epsilon'_{r,cat}$	2.1
Young's modulus of liver; E	10.2 × 10 ⁶ Pa	Electric conductivity of catheter; σ_{cat}	0 S/m
Poisson's ratio of liver; ν	0.48	Relative permeability of catheter; $\mu_{r,cat}$	1
Thermal expansion coefficient of liver; α_{vec}	1 × 10 ⁻⁴ 1/°C	Relative permittivity of slot; $\epsilon'_{r,slot}$	1
Metabolic heat source; Q_{met}	33,800 W/m ³	Electric conductivity of slot; σ_{slot}	0 S/m
		Relative permeability of slot; $\mu_{r,slot}$	1

$$\text{Electric field } (\vec{E}) \quad \vec{E} = e_r \frac{C}{r} e^{j(\omega t - kz)} \quad (1)$$

$$\text{Magnetic field } (\vec{H}) \quad \vec{H} = e_\phi \frac{C}{rZ} e^{j(\omega t - kz)} \quad (2)$$

where $C = \sqrt{ZP/\pi \cdot \ln(r_{outer}/r_{inner})}$, Z is the wave impedance, P is the input microwave power (W), r_{inner} is the dielectric inner radius (m), r_{outer} is the dielectric outer radius (m), $\omega = 2\pi f$ is the angular frequency (rad/s), f is the frequency (Hz), $k = 2\pi/\lambda$ is the propagation constant (m⁻¹) and λ is the wavelength (m).

In the liver tissue, the electric field also has a finite axial component, whereas the magnetic field is purely in the azimuth direction. The electric field is in the radial direction only inside the coaxial cable and in both radial and the axial direction inside the tissue. This allows for the MCA to be modeled using an axisymmetric TM wave formulation. The wave equation then becomes scalar in H_ϕ :

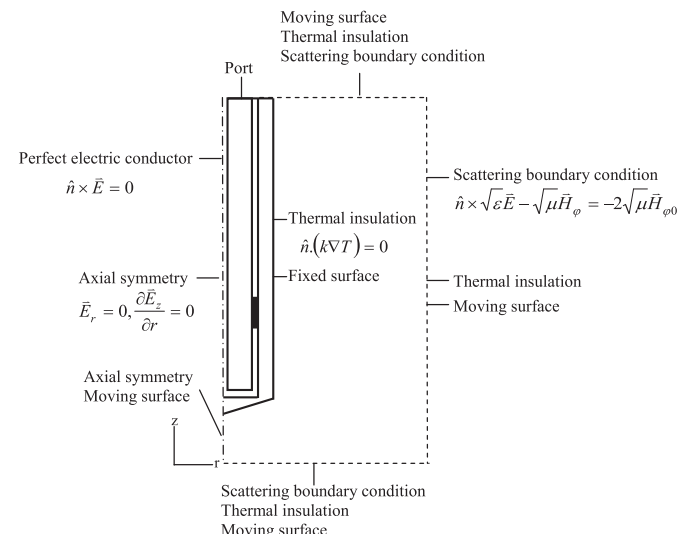


Fig. 3. Boundary conditions for analysis.

$$\nabla \times \left(\left(\epsilon_r' - \frac{j\sigma_{el}}{\omega\epsilon_0} \right)^{-1} \nabla \times \vec{H}_\phi \right) - \mu_r k_0^2 \vec{H}_\phi = 0 \quad (3)$$

where $\epsilon_0 = 8.8542 \times 10^{-12}$ F/m is the permittivity of free space.

The changes in liver tissue dielectric properties are expected to lead to changes in the location of microwave energy deposition within the liver tissue. Dielectric properties changes by gradient of the temperature during MWA. The relative permittivity and conductivity are directly taken from measured to capture changes induced by temperature during thermal ablation [29]. A linear approximation of the dielectric properties is used to estimate the heating rate at temperatures between 37 and 100 °C and is given as following function:

$$\epsilon_{r,liver}'(T) = -0.0424T + 47.043 \quad (4)$$

$$\sigma_{liver}(T) = -0.0004T + 1.7381 \quad (5)$$

Microwave energy is emitted from the MCA slot, which connected to the microwave generator. Microwave energy is propagating through the MCA and into the liver tissue from the MCA slot. Where the boundary conditions for analyzing electromagnetic wave propagation are considered as follows:

At the inlet of the MCA, TM wave propagation with input microwave power of 10 W is considered. An axial symmetry boundary is applied at $r = 0$:

$$\vec{E}_r = 0 \quad (6)$$

$$\frac{\partial \vec{E}_z}{\partial r} = 0 \quad (7)$$

The first order scattering boundary conditions for H_ϕ were used along the outer sides of the liver boundaries to prevent reflection artifacts:

$$\hat{n} \times \sqrt{\epsilon} \vec{E} - \sqrt{\mu} \vec{H}_\phi = -2\sqrt{\mu} \vec{H}_\phi \quad (8)$$

where $\vec{H}_{\phi 0} = C/Zr$ is the excitation magnetic field.

For simplicity and to eliminate numerical error, the inner and outer conductor of the MCA is modeled as the perfect electric conductor (PEC) boundary conditions:

$$\hat{n} \times \vec{E} = 0 \quad (9)$$

3.2. Heat transfer analysis

The heating is illustrated by the temperature distribution estimate, expressed with the bioheat equation, first introduced by Pennes [11]. Pennes's bioheat equation, based on the heat diffusion equation, is a frequency used for analysis of heat transfer in biological tissues [30–32]. The transient bioheat equation effectively describes how heat transfer occurs in liver tissue. The equation can be written as:

$$\rho C \frac{\partial T}{\partial t} = \nabla \cdot (k_{th} \nabla T) + \rho_b C_b \omega_b (T_b - T) + Q_{met} + Q_{ext} \quad (10)$$

where, the left hand side of Eq. (10) denotes the transient term. The first, second, third and fourth terms on the right hand side of Eq. (10) denote heat conduction, heat dissipation by the blood flow, metabolic heat source and external heat source (heat generation by the electric field), respectively.

One could consider that the PTFE catheter is a thermal insulator and the heat transfer analysis is limited to the liver tissue domain; therefore, thermal properties are only needed for liver tissue and blood. The metabolic heat generation rate of 33,800 W/m³ [33,34] is used throughout calculation process. The external heat source is equal to the resistive heat generated by the electromagnetic field (microwave power absorbed) which can be defined as:

$$Q_{ext} = \frac{1}{2} \sigma_{liver} |\vec{E}|^2 \quad (11)$$

The electrical properties strongly affect the temperature increase [35]. When microwave propagates in liver tissue, microwave energy is absorbed by liver tissue and converted into internal heat generation which causes the tissue temperature to rise. The SAR represents the electromagnetic power deposited per unit mass in tissue (W/kg) and is defined by:

$$SAR = \frac{1}{2\rho} \sigma_{liver} |\vec{E}|^2 \quad (12)$$

The SAR distribution is widely used for performance evaluation of heating equipment employed in MWA. Eq. (10) can be rewritten in the form of SAR as:

$$\rho C \frac{\partial T}{\partial t} = \nabla \cdot (k_{th} \nabla T) + \rho_b C_b \omega_b (T_b - T) + Q_{met} + \rho SAR \quad (13)$$

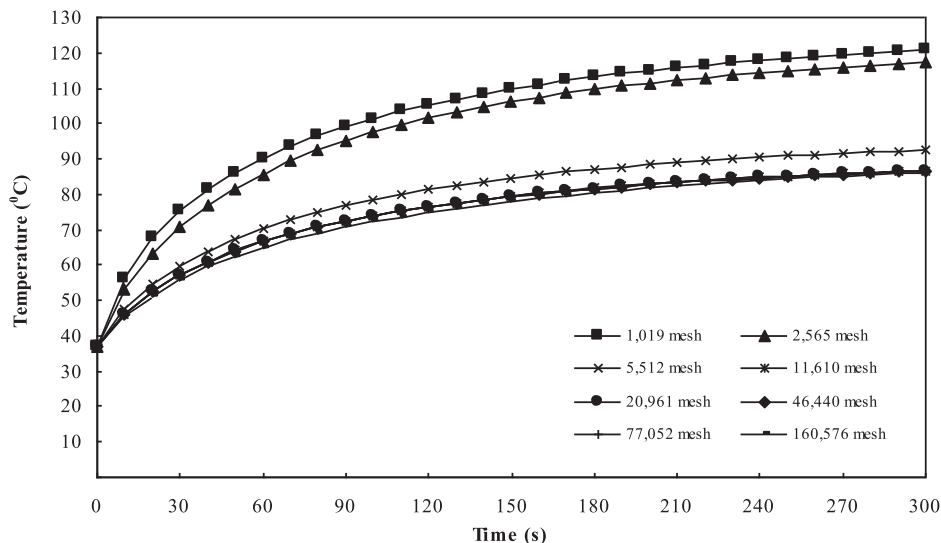


Fig. 4. Relationship between temperature and time from the simulation with the different number of meshes.

Table 3
Computational mesh parameters.

Mesh parameters	Values
Element growth rate	1.3
Maximum element size scaling factor	1
Mesh curvature cut off	0.001
Mesh curvature factor	0.3

Both electromagnetic wave propagation analysis and heat transfer solutions are obtained. The electromagnetic solution is iteratively use as the external heat source of the heat transfer model. In this study, the temperature-dependent properties are considered in calculation procedure. Valvano et al. [36] measured liver tissue thermal conductivity as a function of temperature as shown in following correlation:

$$k_{th}(T) = 0.0012T + 0.4692 \quad (14)$$

Bioheat transfer processes in living tissues are often influenced by the blood perfusion through the vascular network on the local temperature distribution [37]. When there is a significant difference between the temperature of blood and the tissue through which it flows, convective heat transport will occur, altering the temperatures of both the blood and the tissue. Therefore, an understanding of the heat transfer in living tissue must be accounted for the influence of blood perfusion. Where the blood perfusion rate which depends on temperature can be defined as:

$$\omega_b(T) = 0.000021T + 0.00035 \quad (15)$$

For this formulation we have assumed that the change in dielectric and thermal properties is only dependent on tissue temperature. In actuality, it is more complex than this. However, as we stated earlier, we are implementing a model which, while still not complete, is more accurate than the existing thermal model. We will discuss the ramifications of this simplification in the Results and discussion section.

The heat transfer analysis is considered only in the liver tissue domain, which does not include the MCA. The boundaries of the liver tissue are considered as insulating boundary conditions:

$$\hat{n} \cdot (k\nabla T) = 0 \quad (16)$$

Initially, the temperature within the liver tissue is assumed to be uniform:

$$T(t_0) = 37 \text{ }^\circ\text{C} \quad (17)$$

3.3. Mechanical deformation analysis

In this study, liver tissues are considered as an isotropic material. The model is simplified to quasi-static model as presented in several previous studies [38,39]. The physical problem of solid mechanics for an axisymmetric geometry can be described mathematically using the equilibrium equations (equation (18)), the stress–strain relationship (equation (19)) and the strain–displacement relationship (equation (20)) as follows [40]:

$$\frac{\partial \sigma_{rr}}{\partial r} + \frac{\partial \sigma_{rz}}{\partial z} + \frac{\sigma_{rr} - \sigma_{\phi\phi}}{r} + F_r = 0 \quad (18)$$

$$\frac{\partial \sigma_{rz}}{\partial r} + \frac{\partial \sigma_{zz}}{\partial z} + \frac{\sigma_{rz}}{r} + F_z = 0$$

$$\begin{aligned} \epsilon_{rr} &= \frac{1}{E} [\sigma_{rr} - \nu(\sigma_{\phi\phi} + \sigma_{zz})] + \epsilon^{th} \\ \epsilon_{zz} &= \frac{1}{E} [\sigma_{zz} - \nu(\sigma_{\phi\phi} + \sigma_{rr})] + \epsilon^{th} \end{aligned} \quad (19)$$

$$\epsilon_{\phi\phi} = \frac{1}{E} [\sigma_{\phi\phi} - \nu(\sigma_{rr} + \sigma_{zz})] + \epsilon^{th}$$

$$\epsilon_{rz} = \sigma_{rz}(1 + \nu)/E$$

$$\epsilon_{rr} = \frac{\partial u_r}{\partial r}, \quad \epsilon_{zz} = \frac{\partial u_z}{\partial z}, \quad \epsilon_{\phi\phi} = \frac{u}{r} \quad (20)$$

$$\epsilon_{rz} = \frac{1}{2} \left(\frac{\partial u_r}{\partial z} + \frac{\partial u_z}{\partial r} \right)$$

where σ is the stress (Pa), ϵ is the strain, F is the external body load (0 for here), E is Young's modulus (Pa), ν is the Poisson's ratio and u is the average displacement (m). The thermal strain (ϵ^{th}) was calculated as follows:

$$\epsilon^{th} = \int_{T_{ref}}^T \alpha dT \quad (21)$$

where $T_{ref} = 37 \text{ }^\circ\text{C}$ is the reference temperature and α is the temperature-dependent tissue thermal expansion coefficient ($1/^\circ\text{C}$). Equations (18)–(21) describe the thermomechanical behavior of the liver tissue, which is relative to the temperature distribution.

In this study, the liver tissue, connected to the MCA, are set to fixed surface boundary conditions. The outer sides of the liver tissue are set to the moving surface boundary conditions; the tissue is deformed as an effect of thermal strain. In addition, the initial temperature of liver tissue is $37 \text{ }^\circ\text{C}$. And the initial stress and strain are set to zero:

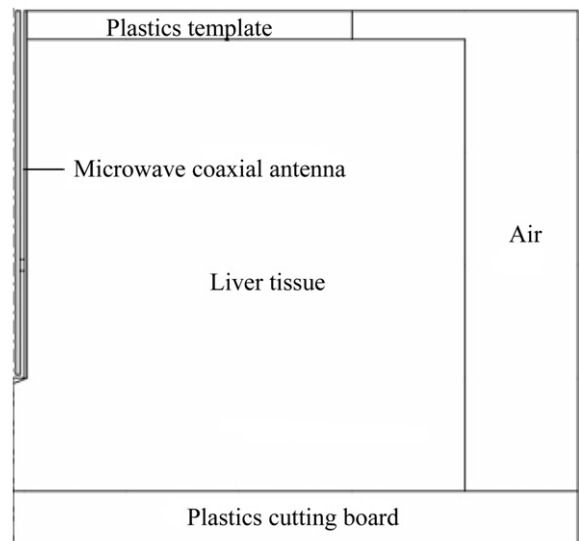


Fig. 5. Geometry of the validation model obtained from the Yang et al.

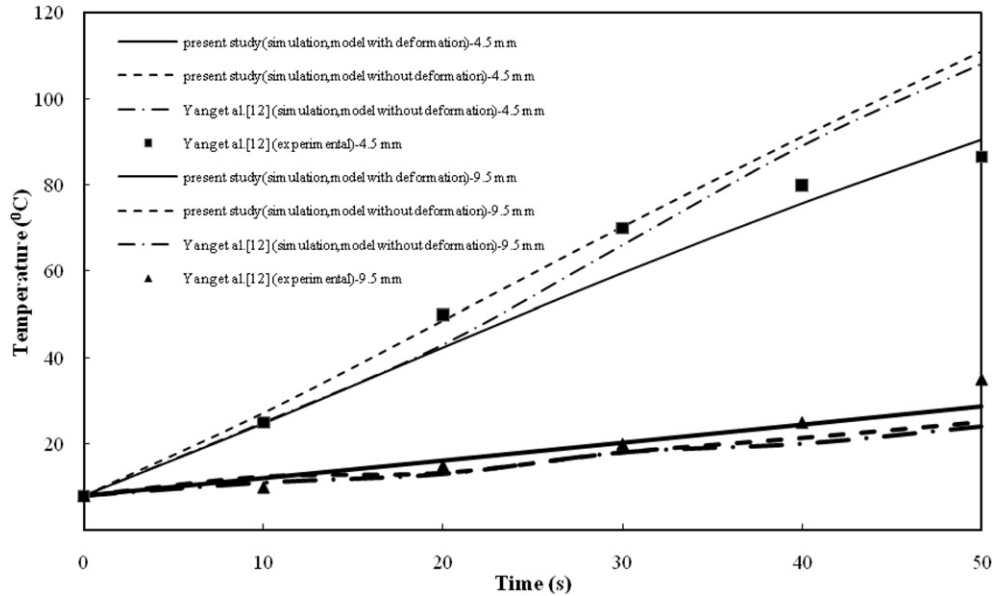


Fig. 6. The validation results of the liver tissue temperature, against Yang et al. (2007).

$$\sigma_{ri}, \sigma_{\phi i}, \sigma_{zi} \text{ and } \sigma_{rzi} = 0 \text{ Pa} \quad (22)$$

$$\epsilon_{ri}, \epsilon_{\phi i}, \epsilon_{zi} \text{ and } \epsilon_{rzi} = 0 \text{ Pa} \quad (23)$$

4. Calculation procedure

In this study, the FEM is used to analyze the transient problems. The computational scheme is to assemble axisymmetric FEM model and compute a local heat generation term by performing an electromagnetic calculation using tissue properties. In order to obtain a good approximation, a fine mesh is specified in the sensitive areas. The coupled equations of electromagnetic wave equation, bioheat equation mechanical deformation equation are solved by the FEM, which was implemented using COMSOL™ Multiphysics 3.4, to demonstrate the phenomenon that occurs within the liver tissue during MWA. The microwave power absorption at each point was computed and used to solve the time-dependent temperature distribution. These temperatures were used to solve the mechanical deformation equation for mechanical behavior of liver tissue, and then the obtained liver tissue deformation was used to recalculate the electromagnetic field and microwave power absorption. Until the steady state is reached, the temperature at each time step is collected.

The axisymmetric FEM model is discretized using triangular element, and the Lagrange quadratic is used to approximate microwave power absorbed, SAR distribution, temperature distribution and strain distribution variation across each element. The convergence test of the frequency of 2.45 GHz is carried out to identify the suitable numbers of element required. The number of elements where solution is independent of mesh density is found to be 11,610. The convergence curve resulting from the convergence test is shown in Fig. 4. Where Fig. 4 shows the relationship between temperature and time from simulations at a critically sensitive point, 2.5 mm away from the antenna and longitudinally aligned with the antenna slot, for different meshes. Computational mesh parameters are shown in Table 3.

5. Results and discussion

5.1. Verification of the model

Fig. 5 shows the geometry of the validation model. In the validation model, the microwave power of 75 W with frequency of 2.45 GHz and the initial liver tissue temperature of 8 °C are selected. The radius of a single slot MCA is 1.25 mm. It is inserted 20 mm deep into liver tissue. The axially symmetrical model is used to analyze the MWA process and the heating time is 50 s. The validity of the numerical scheme is first tested by comparing the present numerical results of model without deformation with existing numerical results [12] under the same condition. The numerical scheme computations are in a very good agreement with the literature results, with error less than 2%. Furthermore, to verify the accuracy of the presented mathematical model of MWA, the resulting data of model with deformation is validated against the experimental results obtained by Yang et al. [12].

Fig. 6 shows the validation results of the liver tissue temperature, with respect to the heating time of 50 s at the positions of 4.5 mm and 9.5 mm away from the MCA. It is found that the simulated results of model with deformation are corresponded closely with the experimental results, whereas the results of model without deformation exhibited errors at both positions.

It is observed that the all cases temperatures of the liver tissue increased with elapsed time, during the MWA process. The results of the simulation of model with deformation reasonable well to

Table 4

Comparisons of RMSE of the liver tissue temperature between the presented study and Yang et al. [12].

Position (mm)	Comparisons of RMSE with experiment from Yang et al. [12], (°C)		
	Presented study (simulation, model with deformation)	Presented study (simulation, model without deformation)	Yang et al. [12] (simulation, model without deformation)
4.5	6.34	12.11	11.03
9.5	2.99	4.95	5.57

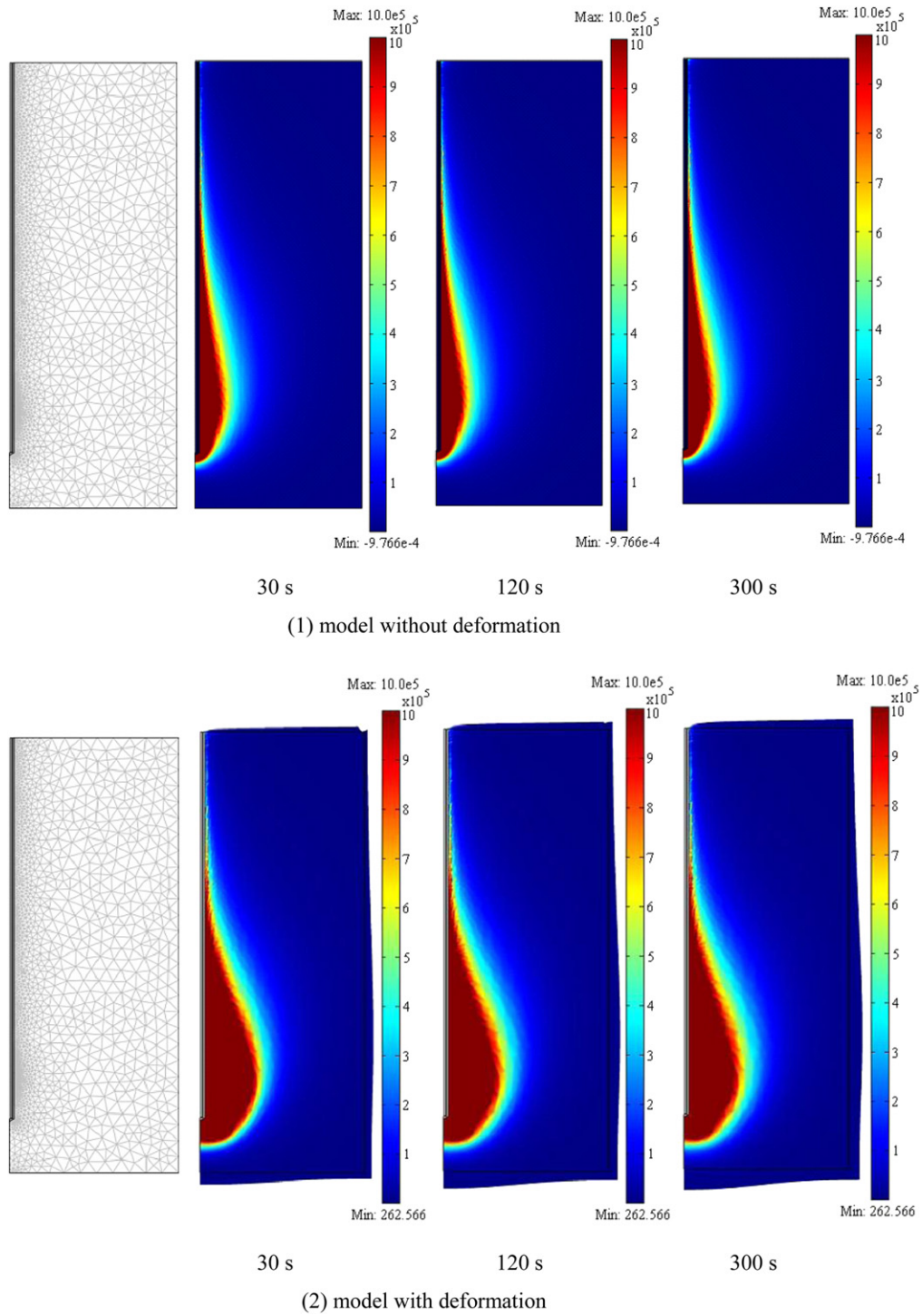


Fig. 7. The microwave power absorbed in liver tissue for various heating times: 30 s, 120 s and 300 s (the scale is cut off at 10^6 W/m^3), (W/m^3).

the experimental results with similar trends in temperature profiles over the same approximate time range. Also, at 9.5 mm the results of the simulation of model with deformation to match the experimental results better. Data from Table 4 shows that the simulated temperature of model without deformation gives greater error than the simulated temperature of model with deformation. In the other words, the model that includes the mechanical deformation behavior of tissue can decrease error of

the simulation. Therefore, the developed model is reliable and can be used for the problem analysis. This is important to obtain the approaching realistic tissues modeling. Certain amounts of mismatch between the simulated results of model with deformation (present study) and the experimental are expected, as [12] has been identified for some dielectric and thermal properties. In addition, the error involved in the simulation is caused by the numerical scheme.

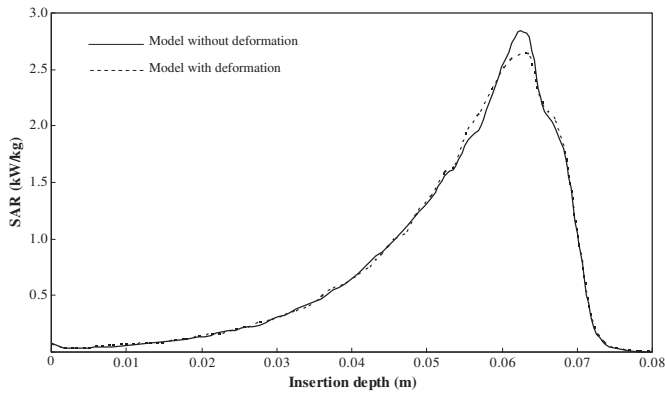


Fig. 8. Comparison of SAR distribution between in model with and without deformation.

5.2. Microwave power absorbed

The basic principle of MWA is to apply microwave power to the liver tissue through the MCA. The microwave energy is absorbed by the liver tissue and heated it. Liver tissue is destroyed after it is heated to a high enough temperature for a sufficiently long time. Fig. 7 shows the simulated results of microwave power absorbed in liver tissues based on a frequency of 2.45 GHz and input microwave power of 10 W. Fig. 7(1) shows the microwave power absorbed in liver tissues in model without deformation and Fig. 7(2) in model with deformation for heating time of 30 s, 120 s, and 300 s, respectively. The figure illustrates the volume heating effect expected from MWA. Microwaves power emitted from the MCA propagates through the liver tissue, which is converted to heat by dielectric heating. According to the results, in both models, the microwave power absorbed distribution is a near ellipsoidal around the slot and its highest values in the vicinity of the slot MCA and decreases with the distance. Where the comparison of the microwave power absorbed between in model with and without deformation, it is found that model with deformation generates a wider microwave power absorbed distribution pattern in liver tissue than model without deformation.

5.3. SAR distribution

Fig. 8 shows the comparison of SAR distribution between in model with and without deformation along a line parallel to the MCA axis with $r = 2.5$ mm which based on a frequency of 2.45 GHz, microwave power of 10 W and heating time of 300 s. In both models, the SAR distributions gradually increase along the longitudinal axis of the MCA to a maximum at the slot exit. In model with deformation, the peak SAR value obtained for 10 W of microwave power is 2.63 kW/kg at the insertion depth approximately of 64 mm close to the slot position. While in model without deformation, the peak SAR value of 2.85 kW/kg is obtained at the insertion depth approximately of 62.5 mm. After that the SAR values quickly decreases and have the lowest value at the insertion depth of 80 mm. Considering the effect of purposed model on the SAR distribution, it can be seen that the model, taking into account the shape deformation, gives a slightly lower peak SAR value than the model without deformation. The peak SAR value differences for the two models are 8.37%. However, there is no clear difference between these two models, due to the low microwave power input from the MCA, and the slightly changing tissue density between heating. In both models, the SAR pattern fluctuates due to the interference of electromagnetic wave propagation from MCA.

Moreover, these results in both models correspond with a previous study by Saito et al. [17]. It is found that the variation of SAR distribution in the liver tissue due to different model assumption is performed.

5.4. Temperature distribution

Fig. 9 shows the simulated results of temperature distribution in liver tissues based on a frequency of 2.45 GHz and microwave power of 10 W. Fig. 9(1) shows the temperature distribution in liver tissues in model without deformation and Fig. 9(2) in model with deformation for heating time of 30 s, 120 s, and 300 s, respectively. The microwave power absorbed is stronger near the tip and the slot of the MCA (as shown in Fig. 7), leads to a high temperature at near the tip and the slot of the MCA slot. In both models, the temperature distribution forms a nearly ellipsoidal distribution around the slot and its highest values in the vicinity of the slot MCA and decreases with the distance. That is probably because the thermal stress overwhelms mechanical stress in this particular model. The temperature increases rapidly in the early time of heating, reaches a peak value, and then decreases gradually towards steady state. That is because the microwave power absorbed within the liver tissue attenuates owing to energy absorption, and thereafter the absorbed energy is converted to the thermal energy, which increases the tissue temperature. In addition, the temperature distribution is related to heating time and deformation of liver tissue. The obtained results show that the maximum temperature increase is capable of destroying cancer in liver tissue (cancer cells start to die at about 50 °C). Comparison of the temperature distribution in both models, which correspond with the microwave power absorbed is shown in Fig. 7. For the model without deformation, the temperature profile within the liver tissue (Fig. 9(1)) displays a strong ellipsoidal distribution, corresponding to the microwave power absorbed (Fig. 7(1)). This is because the microwave power absorbed within the liver tissue attenuates, owing to energy absorption, and thereafter the absorbed energy is converted into thermal energy, which increases the liver temperature. In this model, the temperature distribution is not influenced by the thermal strain effect. It is found that the temperature decays quickly along the propagation direction following the microwave power absorbed. The maximum temperature within the sample is around 93.445 °C at heating time of 300 s.

For the MWA of liver tissue in model with deformation, the simulations of the temperature distribution are shown in Fig. 9(2). The temperature profile within the liver tissue also displays a strong ellipsoidal distribution, corresponding to the microwave power absorbed (Fig. 7(2)), as same as the results of the model without deformation. Since the high temperature in liver tissue leads to tissue deformation due to the correlation of thermal and mechanical properties of tissue, the temperature decays much more slowly compared to that in the model without deformation. In this model, the temperature distribution is influenced by the thermal strain effects. Therefore, the temperature field decreases slowly along the propagating direction. It is evident from Fig. 9(2) that, in this model, there is only one peak appearing in the temperature distribution. The maximum temperature within the sample is around 92.724 °C at heating time of 300 s.

Considering the comparison of the purposed models based on the maximum temperature, it can be seen that the model, taking into account the shape deformation, gives a slightly lower maximum temperature than the model without deformation. The maximum temperature differences for the two models are about 0.778%, which based on a frequency of 2.45 GHz, microwave power of 10 W and heating time of 300 s. This is because the penetration area of microwave of liver tissue in the model without deformation

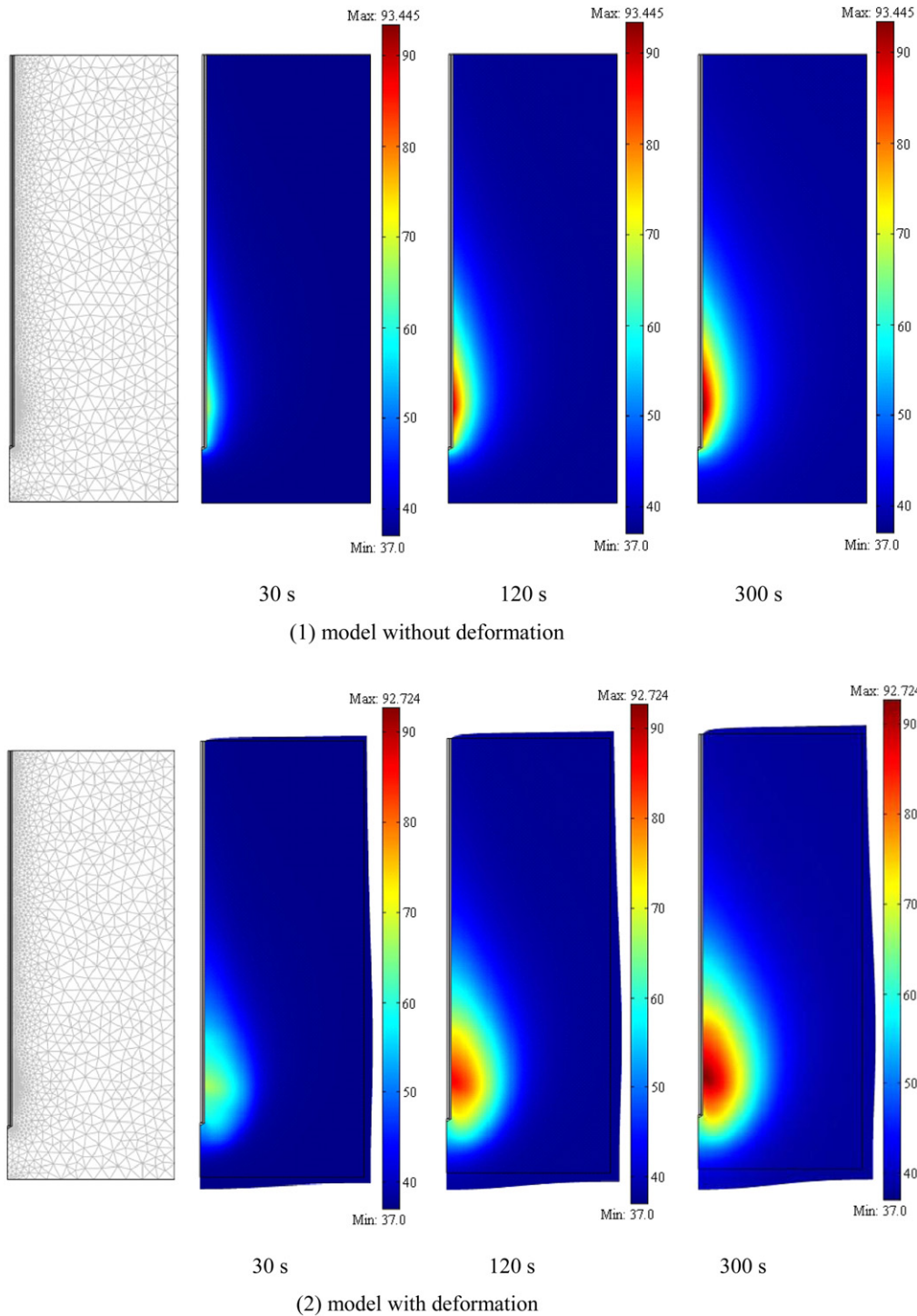


Fig. 9. The temperature distribution in liver tissue for various heating times: 30 s, 120 s and 300 s (°C).

is smaller than the penetration area of microwave of liver tissue in the model with deformation. Therefore, the maximum temperature of liver tissue in model without deformation is slightly higher than the maximum temperature of liver tissue in the model with deformation.

Fig. 10 shows the comparison of the four position temperature curves at the slot center (the insertion depth of 64 mm) of the model with and without deformation versus time. The results of both models show similar trends of temperature distribution that is

the temperature increases rapidly in the early time of heating and approach to steady state at increasing heating time. The temperatures difference at the heating time of 300 s for the two models is about 0.482% at the position of 1 mm, 0.405% at the position of 2 mm, 0.278% at the position of 4 mm, and 0.099% at the position of 8 mm, respectively. It is observed that the liver tissue temperature is high at the position close to the antenna slot. The temperature difference between two models obviously occurs at the hot spot zone, due to the higher effect of mechanical deformation. However,

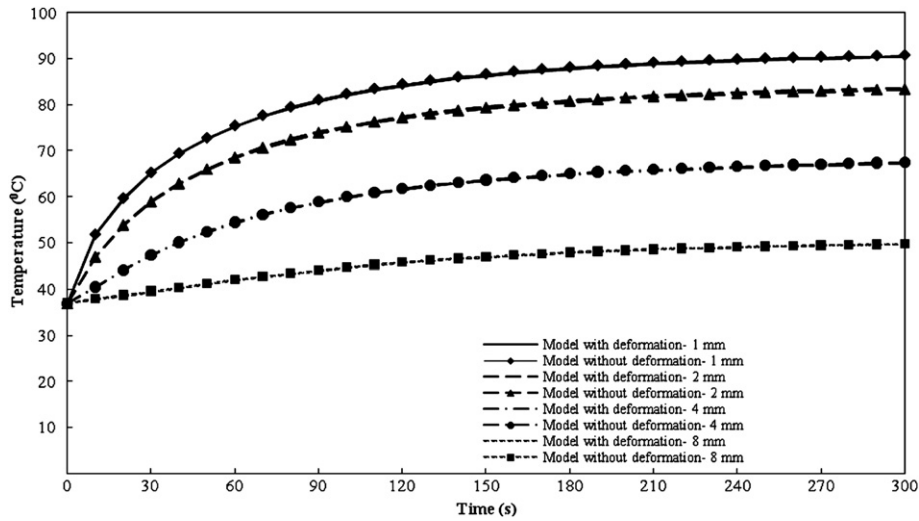


Fig. 10. Comparison of the four position temperature curves at the slot center (the insertion depth of 64 mm) of the model with and without deformation versus time.

the severity of the resultant physiological effects produced by small temperature increases, as well as mechanical deformation, can be expected to worsen in sensitive organs. Therefore, for effective treatment, the using of model including mechanical deformation is recommended to represent actual behavior of tissue during MWA.

5.5. Strain distribution

During MWA, temperature gradient will be occurred within the liver tissue which leads to non-uniform thermal strain inside the liver. This mechanical deformation influences the behavior of heat transfer within liver tissue. Fig. 11 shows the simulated results of normal strain distribution in liver tissue based on a frequency of 2.45 GHz, microwave power of 10 W and heating time of 30 s, 120 s, and 300 s, respectively. It is found that high strain distribution

occurs in the region near the MCA slot, and then decreases with distance from the MCA due to the SAR distribution effect. In addition, the normal strain distribution is also presented at the boundary of the liver tissue and this strain causing an effect on the SAR and on the temperature distribution. This means that the thermally induced deformation of tissue may play a role in the MWA process of any tissues, which however it is not taken into account the current MWA treatments study.

Fig. 12 shows the comparison of four position strain curves at the slot center (the insertion depth of 64 mm) where the model with deformation versus time. It is found that the strain increases rapidly in the early time of heating, reaches a peak value, and then decreases gradually toward steady state. In addition, the liver tissue at the position of 1 mm displays a highest strain, followed by the positions of 2 mm, 4 mm and 8 mm, respectively. It is observed that

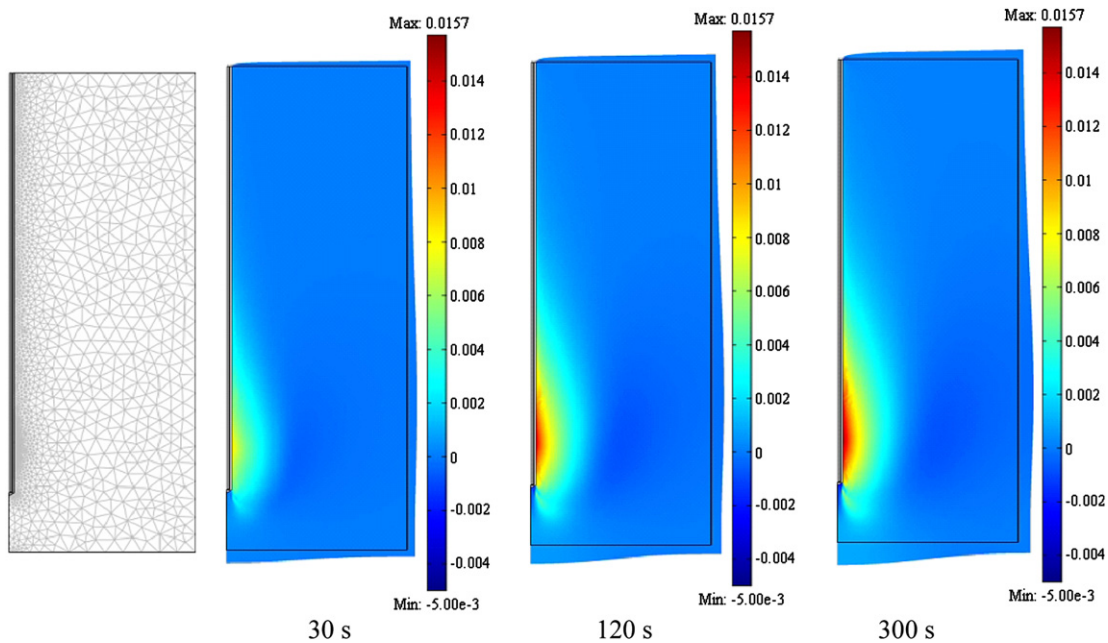


Fig. 11. The strain distribution in liver tissue in model with deformation for various heating times: 30 s, 120 s and 300 s.

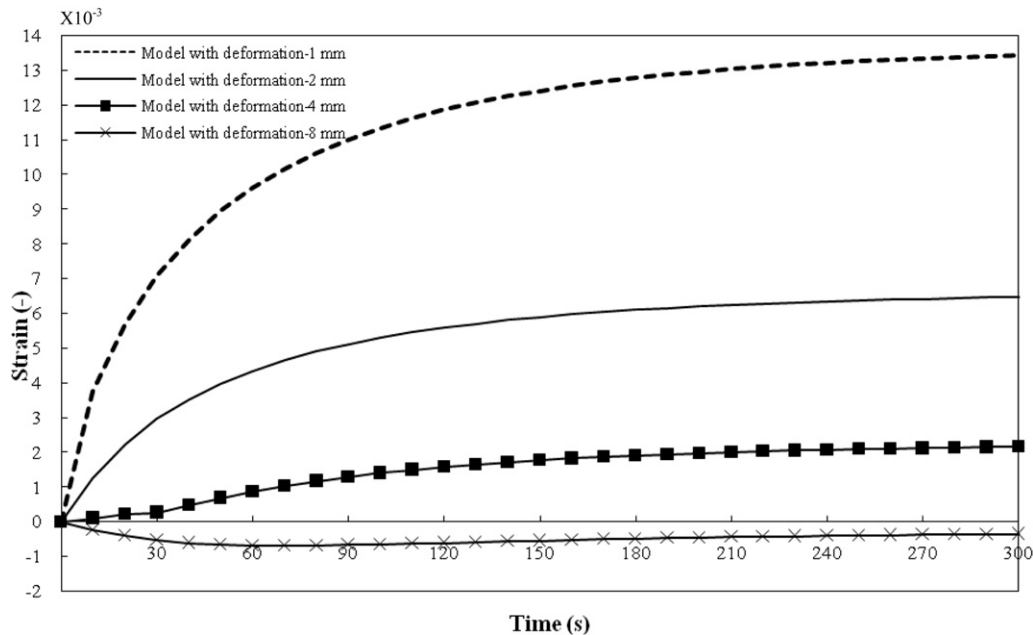


Fig. 12. The comparison of four position strain curves at the slot center (the insertion depth of 64 mm) where the model with deformation versus time.

the strain profiles show the similar trend of temperature profiles, over the same approximation time range. All positions show a positive strain, except at the position of 8 mm, in which a negative value is shown. This is a negative strain, as it denotes the tissue shrinkage. It can be concluded that, the liver tissue near the MCA will be influenced by temperature distribution than the liver tissue far away from the MCA. This will affect the heat transfer within the liver tissue.

6. Conclusion

Clinical treatment with MWA needs an accurate control of the lesion generation in order to ensure cancer tissue destruction and to minimize damage to normal liver tissue. Computer simulation is necessary to optimize the MWA procedure. For effective treatment, a model that represents the complete mathematical model considered electromagnetic wave propagation, heat transfer and mechanical deformation of biological tissue is needed. In this work, the model with and without deformation is carried out in order to compare their effects on the microwave power absorbed, SAR distribution, temperature distribution and strain distribution in liver tissue. The developed models from this work have enabled us to get more accurate predictions during MWA using an MCA. In addition, the simulated results in this study can be used as a guideline for the practical treatment.

In next step of research, the formulation of 3D modeling for approaching realistic liver tissue will be performed. Current work has already done to simulate the MWA in tissue where this tissue is modeled as a porous media base. During the MWA process, tissue will lose water content due to the generation of water vapor, and tissue will perform multiphase flow behavior in unsaturated hygroscopic porous media [41]. In this consideration, the capillary pressure and vapor diffusion influences the MWA process, where realistic behavior is approached.

Acknowledgements

The authors gratefully acknowledge the financial support this work provided by Thammasat University and the Thailand Research

Fund (TRF) under the Royal Golden Jubilee Ph.D. Program (RGJ) Contract No. PHD/0362/2551.

References

- [1] S. Chatterjee, T. Basak, S.K. Das, Microwave driven convection in a rotating cylindrical cavity: a numerical study, *Journal of Food Engineering* 79 (2007) 1269–1279.
- [2] W. Cha-um, P. Rattanadecho, W. Pakdee, Experimental and numerical analysis of microwave heating of water and oil using a rectangular waveguide: influence of sample sizes, positions and microwave power, *Food and Bioprocess Technology* 4 (4) (2011) 544–558.
- [3] M.A. Abdelghani-Idrissi, Experimental investigations of occupied volume effect on the microwave heating and drying kinetics of cement powder in a mono-mode cavity, *Applied Thermal Engineering* 9 (2001) 955–965.
- [4] P. Rattanadecho, K. Aoki, M. Akahori, The characteristics of microwave melting of frozen packed bed using a rectangular waveguide, *IEEE Transaction of Microwave Theory and Techniques* 50 (6) (2002) 1495–1502.
- [5] K. Jeni, M. Yapa, P. Rattanadecho, Design and analysis of the commercialized drier processing using a combined unsymmetrical double-feed microwave and vacuum system (case study: tea leaves), *Chemical Engineering and Processing: Process Intensification* 49 (2010) 389–395.
- [6] J.F. McGahan, G.D. Dodd III, Radiofrequency ablation of the liver: current status, *American Journal of Roentgenology* 176 (1) (2001) 3–16.
- [7] W.Y. Lau, T.W.T. Leung, S.C.H. Yu, Percutaneous local ablative therapy for hepatocellular carcinoma: a review and look into the future, *Annals of Surgery* 237 (2) (2003) 171–179.
- [8] Ablative techniques (percutaneous) thermal ablative techniques. in: T.J. Vogl, T.K. Helmlinger, M.G. Mack, M.F. Reiser (Eds.), *Percutaneous Tumor Ablation in Medical Radiology*, Springer, Berlin, Germany, (2008) 7–32.
- [9] S. Garrean, J. Hering, A. Saied, et al., Ultrasound monitoring of a novel microwave ablation (MWA) device in porcine liver: lessons learned and phenomena observed on ablative effects near major intrahepatic vessels, *Journal of Gastrointestinal Surgery* 13 (2) (2009) 334–340.
- [10] A.U. Hines-Peralta, N. Pirani, P. Clegg, N. Cronin, T.P. Ryan, Z. Liu, S.N. Goldberg, Microwave ablation: results with a 2.45-GHz applicator in ex vivo bovine and in vivo porcine liver, *Radiology* 239 (1) (2006) 94–102.
- [11] H.H. Pennes, Analysis of tissue and arterial blood temperatures in the resting human forearm, *Journal of Applied Physiology* 85 (1) (1998) 5–34.
- [12] D. Yang, M. Converse, D. Mahvi, Expanding the bioheat equation to include tissue internal water evaporation during heating, *IEEE Transactions on Biomedical Engineering* 54 (8) (2007) 1382–1388.
- [13] J. Okajima, S. Maruyama, H. Takeda, Dimensionless solutions and general characteristics of bioheat transfer during thermal therapy, *Journal of Thermal Biology* 34 (8) (2009) 377–384.
- [14] K.J. Chua, S.K. Chou, On the study of the freeze-thaw thermal process of a biological system, *Applied Thermal Engineering* 29 (17–18) (2009) 3696–3709.
- [15] T. Wessapan, S. Srisawatthisukul, P. Rattanadecho, The effects of dielectric shield on specific absorption rate and heat transfer in the human body

- exposed to leakage microwave energy, International Communications in Heat and Mass Transfer 38 (2) (2011) 255–262.
- [16] T. Wessapan, S. Srisawatdhisukul, P. Rattanadecho, Numerical analysis of specific absorption rate and heat transfer in the human body exposed to leakage microwave power at 915 MHz and 2450 MHz, Journal of Heat Transfer 133 (5) (2011) art. no. 051101.
- [17] K. Saito, S. Hosaka, S.Y. Okabe, A proposition on improvement of a heating pattern of an antenna for microwave coagulation therapy: introduction of a coaxial-dipole antenna, Electronics and Communications in Japan, Part I: Communications (English translation of Denshi Tsushin Gakkai Ronbunshi) 86 (1) (2003) 16–23.
- [18] P. Keangin, P. Rattanadecho, T. Wessapan, An analysis of heat transfer in liver tissue during microwave ablation using single and double slot antenna, International Communications in Heat and Mass Transfer 38 (2011) 757–766.
- [19] S. Tungjitkusolmun, S.T. Staelin, D. Haemmerich, J.Z. Tsai, H. Cao, J.G. Webster, et al., Three-dimensional finite-element analyses for radio-frequency hepatic tumor ablation, IEEE Transactions on Biomedical Engineering 49 (2002) 3–9.
- [20] W. Shen, J. Zhang, F. Yang, Modeling and numerical simulation of bioheat transfer and biomechanics in soft tissue, Mathematical and Computer Modelling 41 (11–12) (2005) 1251–1265.
- [21] F. Xu, T. Wen, T.J. Lu, Skin biothermomechanics for medical treatments, Journal of the Mechanical Behavior of Biomedical Materials 1 (2) (2008) 172–187.
- [22] D.S. Moran, U. Eliyahu, Y. Heled, S. Rabinovitz, J. Hoffman, M. Margalot, Core temperature measurement by microwave radiometry, Journal of Thermal Biology 29 (2004) 539–542.
- [23] C.P. Lau, Y.T. Tai, P.W. Lee, The effects of radiofrequency ablation versus medical therapy on the quality-of-life and exercise capacity in patients with accessory pathway-mediated supraventricular tachycardia: a treatment comparison study, PACE – Pacing and Clinical Electrophysiology 18 (31) (1995) 424–432.
- [24] J.P. McGahan, J.M. Brock, H. Tesluk, W.Z. Gu, P. Schneider, P.D. Browning, Hepatic ablation with use of radio-frequency electrocautery in the animal model, Journal of Vascular and Interventional Radiology 3 (2) (1992) 291–297.
- [25] J.M. Bertram, D. Yang, M.C. Converse, Antenna design for microwave hepatic ablation using an axisymmetric electromagnetic model, Bio-Medical Engineering Online 5 (2006).
- [26] D. Yang, J.M. Bertram, M.C. Converse, et al., A floating sleeve antenna yields localized hepatic microwave ablation, IEEE Transactions on Biomedical Engineering 53 (3) (2006) 533–537.
- [27] S. Jacobsen, P.R. Stauffer, Can we settle with single-band radiometric temperature monitoring during hyperthermia treatment of chestwall recurrence of breast cancer using a dual-mode transceiving applicator? Physics in Medicine and Biology 52 (4) (2007) 911–928.
- [28] M. Cepeda, A. Vera, L. Leija, et al., Coaxial double slot antenna design for interstitial hyperthermia in muscle using a finite element computer modeling, In: IEEE International Instrumentation and Measurement Technology Conference I2MTC (2008) 961–963.
- [29] C.L. Brace, Temperature-dependent dielectric properties of liver tissue measured during thermal ablation: toward an improved numerical model, In: Conference Proceedings: Annual International Conference of the IEEE Engineering in Medicine and Biology Society (2008) 230–233.
- [30] H. Arkin, Recent developments in modeling heat transfer in blood perfused tissues, IEEE Transactions on Biomedical Engineering 41 (2) (1994) 97–107.
- [31] E.H. Wissler, Pennes's 1948 paper revisited, Journal of Applied Physiology 85 (1998) 35–41.
- [32] A. Shitzer, R.C. Eberhart, Heat Transfer in Biology and Medicine. Plenum Press, New York, 1985.
- [33] J. Lienhard, A Heat Transfer Textbook. Phlogiston, Lexington, MA, 2005.
- [34] Y. Rabin, A. Shitzer, Numerical solution of the multidimensional freezing problem during cryosurgery, Journal Biomechanical Engineering 120 (1) (1998) 32–37.
- [35] M. Fujimoto, A. Hirata, J. Wang, et al., FDTD-derived correlation of maximum temperature increase and peak SAR in child and adult head models due to dipole antenna, IEEE Transactions on Electromagnetic Compatibility 48 (1) (2006) 240–247.
- [36] J.W. Valvano, J.R. Cochran, K.R. Diller, Thermal conductivity and diffusivity of biomaterials measured with self-heated thermistors, International Journal of Thermophysics 6 (3) (1985) 301–311.
- [37] J. Shi, Z. Chen, M. Shi, Simulation of heat transfer of biological tissue during cryosurgery based on vascular trees, Applied Thermal Engineering 29 (8–9) (2009) 1792–1798.
- [38] B. Rubinsky, Thermal stress during Solidification processes, ASME Journal of Heat Transfer 104 (1982) 196–199.
- [39] S. Lin, D.Y. Gao, X.C. Yu, Thermal stress induced by water solidification in a cylindrical tube, ASME ASME Journal of Heat Transfer 112 (1990) 1079–1082.
- [40] B.A. Boley, J.H. Weiner, Theory of Thermal Stress. Wiley, New York, 1960.
- [41] P. Rattanadecho, K. Aoki, M. Akahori, Influence of irradiation time, particle sizes, and initial moisture content during microwave drying of multi-layered capillary porous materials, Journal of Heat Transfer 124 (1) (2002) 151–161.

Nomenclature

C : heat capacity of liver tissue (J/kg °C)
 C_b : heat capacity of blood (J/kg °C)
 E : Young's modulus (Pa)
 \vec{E} : electric field (V/m)
 F : external body load (N)
 f : microwave frequency (Hz)
 \vec{H} : magnetic field (A/m)
 $\vec{H}_{\phi 0}$: excitation magnetic field (A/m)
 k : propagation constant (m^{-1})
 k_{th} : thermal conductivity of liver tissue (W/m °C)
 k_0 : propagation constant of free space (m^{-1})
 P : input microwave power (W)
 Q_{ext} : external heat source (W/m³)
 Q_{met} : metabolism heat source (W/m³)
 r_{inner} : dielectric inner radius (m)
 r_{outer} : dielectric outer radius (m)
 T : actual temperature (°C)
 T_b : temperature of blood (°C)
 T_{ref} : reference temperature (°C)
 t : time (s)
 u : average displacement (m)
 Z : wave impedance in the dielectric of the coaxial cable (Ω)

Greek symbols

ρ : density of liver tissue (kg/m³)
 ρ_b : density of blood (kg/m³)
 λ : wavelength (m)
 ω : angular frequency (rad/s)
 ω_b : blood perfusion rate (1/s)
 ϵ : strain
 ϵ_0 : permittivity of free space (F/m)
 ϵ_r : relative permittivity (–)
 σ_{el} : electric conductivity (S/m)
 σ : stress (Pa)
 σ_{liver} : electric conductivity of liver (S/m)
 μ : permeability (H/m)
 μ_r : relative permeability (–)
 ν : poisson's ratio
 α : thermal expansion coefficient (1/°C)

Subscripts

b : blood
 el : electric
 ext : external
 i : initial
 $inner$: inner
 $liver$: liver
 met : metabolism
 $outer$: outer
 r : relative
 ref : reference
 $r, z, \text{ and } \phi$: components of cylindrical coordinates
 0 : free space

Superscripts

th : thermal